The adhesion modulation domain of *Caenorhabditis elegans* α-catenin regulates actin binding during morphogenesis

Xiangqiang Shao[a,†], Bethany Lucas[b], Jared Strauch[c], and Jeff Hardin[a,c,*]
[a]Program in Genetics and [c]Department of Integrative Biology, University of Wisconsin–Madison, Madison, WI 53706;
[b]Department of Biology, Regis University, Denver, CO 80221

ABSTRACT **Maintaining tissue integrity during epidermal morphogenesis depends on α-catenin, which connects the cadherin complex to F-actin. We show that the adhesion modulation domain (AMD) of *Caenorhabditis elegans* HMP-1/α-catenin regulates its F-actin–binding activity and organization of junctional–proximal actin in vivo. Deleting the AMD increases F-actin binding in vitro and leads to excess actin recruitment to adherens junctions in vivo. Reducing actin binding through a compensatory mutation in the C-terminus leads to improved function. Based on the effects of phosphomimetic and nonphosphorylatable mutations, phosphorylation of S509, within the AMD, may regulate F-actin binding. Taken together, these data establish a novel role for the AMD in regulating the actin-binding ability of an α-catenin and its proper function during epithelial morphogenesis.**

Monitoring Editor
Richard Fehon
University of Chicago

Received: Jan 9, 2019
Revised: May 28, 2019
Accepted: Jun 4, 2019

INTRODUCTION

Stable intercellular adhesions mediated by a highly conserved cadherin–catenin complex (CCC) play key roles in maintaining tissue integrity during metazoan embryonic development (Harris and Tepass, 2010; Takeichi, 2014). The intracellular tail of cadherin binds to β-catenin (Ozawa *et al.*, 1989); α-catenin binds β-catenin and physically links the CCC at the membrane to the F-actin cytoskeleton (Pokutta and Weis, 2000; Pokutta *et al.*, 2002; Buckley *et al.*, 2014).

α-Catenin is an actin-binding and -bundling protein with three vinculin homology domains (Herrenknecht *et al.*, 1991). The N-termini of mammalian αE- and αN-catenin contain overlapping β-catenin–binding and homodimerization sites (Pokutta and Weis, 2000; Pokutta *et al.*, 2014); the C-terminus contains the actin-binding domain (ABD; Imamura *et al.*, 1999; Pokutta *et al.*, 2002). αE-Catenin is regulated in several ways: 1) αE-catenin homodimers have a higher affinity for F-actin than do αE-catenin–β-catenin heterodimers (Drees *et al.*, 2005; Rangarajan and Izard, 2013); 2) the affinity of αE-catenin for F-actin is regulated by whether the actin is under tension (Buckley *et al.*, 2014); 3) the first α-helical region of the ABD may regulate the affinity of the ABD for F-actin (Ishiyama *et al.*, 2018); and 4) the middle (M) domain, composed of three helical bundles designated M1, M2, and M3 (Ishiyama *et al.*, 2013) contains a vinculin-binding site (Watabe-Uchida *et al.*, 1998; Choi *et al.*, 2012) buried by M2 and M3 when αE-catenin is not under tension (Yonemura *et al.*, 2010; Choi *et al.*, 2012; Rangarajan and Izard, 2012; Ishiyama *et al.*, 2013; Thomas *et al.*, 2013).

Further functional investigation of the M domain, especially in vivo, is warranted. The functional importance of vinculin binding remains unclear, because deletion of the relevant region within M1 does not lead to striking changes in cultured cells (Huveneers *et al.*, 2012), and constructs lacking the VH2 domain in *Drosophila* are capable of rescuing α-catenin null border cells or embryos to a significant extent (Desai *et al.*, 2013). We decided to focus on the adhesion modulation domain (AMD), comprising residues 509–643 of αE-catenin, which correspond to the M3 domain plus the linker region between M3 and the ABD (Figure 1A). The αE-catenin AMD supports lateral clustering of cadherins and nascent junction formation in cultured cells (Imamura *et al.*, 1999) and it serves as a docking

This article was published online ahead of print in MBoC in Press (http://www.molbiolcell.org/cgi/doi/10.1091/mbc.E19-01-0018) on June 12, 2019.

X.S. and J.H. conceptualized the study; formal analysis was performed by X.S., B.L., and J.H.; funding acquisition was by J.H.; investigation was performed by X.S., B.L., and J.S.; the methodology was designed by X.S., B.L., and J.H.; J.H. was responsible for project administration; resources were provided by X.S., I.C.S., W.B., K.K., D.R., and J.H.; supervision was carried out by J.H.; validation was performed by X.S., B.L., J.S., and J.H.; visualization was by X.S. and J.H.; writing of the original draft was by X.S.; review and editing was done by X.S., B.L., and J.H.

†Present address: Wisconsin State Laboratory of Hygiene, University of Wisconsin–Madison, Madison, WI 53706.

*Address correspondence to: Jeff Hardin (jdhardin@wisc.edu).

Abbreviations used: ABD, actin-binding domain; AMD, adhesion modulation domain; CCC, cadherin–catenin complex; CFB, circumferential filament bundles; DIC, differential interference contrast; GFP, green fluorescent protein; PBST, phosphate-buffered saline + 0.1% Tween-20.

© 2019 Shao *et al*. This article is distributed by The American Society for Cell Biology under license from the author(s). Two months after publication it is available to the public under an Attribution–Noncommercial–Share Alike 3.0 Unported Creative Commons License (http://creativecommons.org/licenses/by-nc-sa/3.0).

"ASCB®," "The American Society for Cell Biology®," and "Molecular Biology of the Cell®" are registered trademarks of The American Society for Cell Biology.

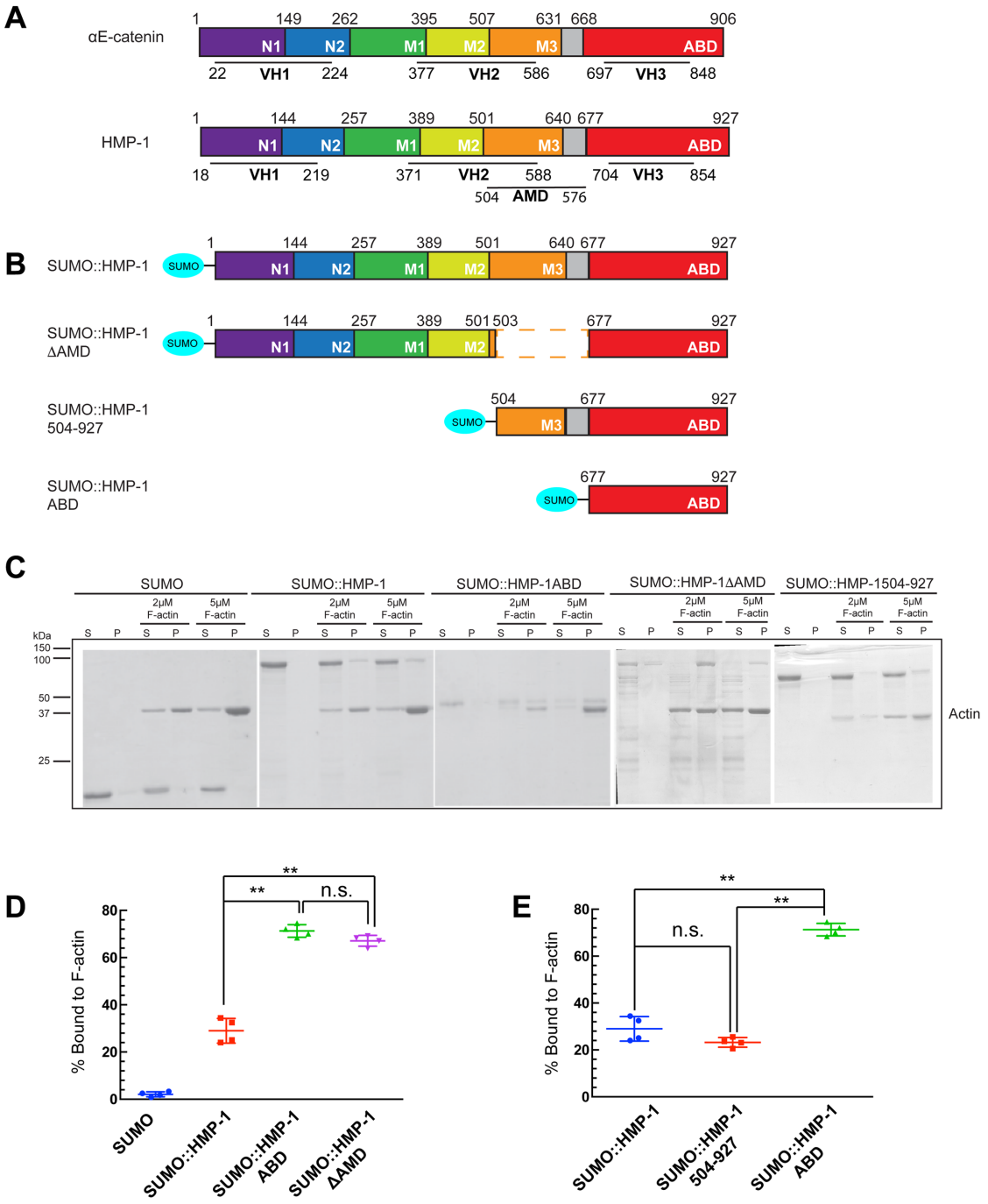

FIGURE 1: The adhesion modulation domain (AMD) of HMP-1 regulates F-actin binding. (A) Domain structure of HMP-1 and αE-catenin. Each domain boundary is labeled with residue numbers. Both HMP and αE-catenin include three vinculin homology domains (VH1-3) and two N-terminal subdomains (N1 and N2). The middle of the protein (M domain) is composed of three subdomains (M1, M2, and M3). The actin-binding domain (ABD) lies at the C-terminus. (B) Schematics of the protein constructs used in the actin cosedimentation assays. (C) Coomassie-stained SDS–PAGE gels of actin cosedimentation experiments. S = supernatant fraction, P = pellet fraction. (D) Quantification of data from C. The percentage of protein in the pellet fraction was compared at 5 μM F-actin. Error bars represent mean ± SEM ($n = 4$). (**, $p \leq 0.01$; n.s., not significant; Student's t test). (E) Quantification of data from actin cosedimentation experiments for SUMO::HMP-1504-927, SUMO::HMP-1, and SUMO::HMP-1ABD. Error bars represent mean ± SEM ($n = 4$) (**, $p \leq 0.01$; n.s., not significant; Student's t test).

site for other actin-binding proteins such as afadin (Mandai *et al.*, 1997; Pokutta *et al.*, 2002). Phosphorylation and dephosphorylation of the phospho-linker (P-linker) region within the AMD is required for normal α-catenin function, although the underlying mechanism is unclear (Escobar *et al.*, 2015).

Caenorhabditis elegans provides a unique model to study the function of the AMD in vivo. *C. elegans* is amenable to genetic manipulation, visualization of morphogenetic movements, and it has single conserved homologues of core CCC components (Costa *et al.*, 1998; Pettitt *et al.*, 2003). HMP-1/α-catenin possesses a canonical M

domain (Kang *et al.*, 2017), but is incapable of forming homodimers (Kwiatkowski *et al.*, 2010; Callaci *et al.*, 2015; Kang *et al.*, 2017).

We show here that the AMD negatively regulates F-actin binding of HMP-1 and that S509 within the AMD, which is endogenously phosphorylated (Callaci *et al.*, 2015), is important for proper function of HMP-1 during embryonic development. We also show that the N-terminus of the HMP-1 ABD is required for its full actin-binding ability. These results identify novel roles for the AMD and the adjacent C-terminal region in a biologically relevant context.

RESULTS AND DISCUSSION

The HMP-1 AMD negatively regulates F-actin binding

We sought an internal domain within HMP-1 that might be responsible for negative regulation of the full-length protein. To this end, we generated a series of internal deletions of recombinant SUMO::HMP-1 and used these in actin cosedimentation experiments (Figure 1B). Consistent with our previous findings (Kang *et al.*, 2017), full-length recombinant HMP-1 (HMP-1FL) cosedimented with F-actin. Surprisingly, however, it did so to a markedly lesser extent than the C-terminus alone (Figure 1, C and D). Significantly, deletion of the AMD increased F-actin binding to nearly the same level as the isolated HMP-1 C-terminus, indicating that the AMD is necessary for negative regulation of full-length HMP-1 (Figure 1, C and D). We next tested the sufficiency of the AMD for negative regulation. HMP-1 constructs lacking the N-terminus and the N-terminal portion of the M domain but retaining the AMD (aa504–927) exhibited F-actin binding comparable to HMP-1FL (Figure 1E); thus, the AMD appears to be necessary and sufficient to confer intramolecular autoinhibition on the HMP-1 C-terminus.

The HMP-1 AMD is important for normal F-actin recruitment to adherens junctions

That the AMD regulated HMP-1 binding to F-actin in vitro led us to investigate the role of the AMD in vivo. Previous studies used a deletion allele, *hmp-1(zu278)*, which encodes a protein that retains part of the N-terminus and M domain of HMP-1 (Costa *et al.*, 1998; Kwiatkowski *et al.*, 2010; Maiden *et al.*, 2013). To avoid possible complexities in analysis, we generated a new null mutant allele, *hmp-1(jc48)*, via CRISPR (Supplemental Figure S1), and assessed the ability of transgenes encoding various GFP-tagged HMP-1 deletions to rescue lethality in *hmp-1(jc48)* homozygotes. Expression levels of rescuing transgenes were found to be essentially identical (Supplemental Figure S2).

Full-length HMP-1::GFP fully rescues *hmp-1(jc48)* mutants (Figure 2A); rescued mutants develop indistinguishably from wild type. We next investigated the function of HMP-1::GFP lacking the AMD. HMP-1ΔAMD::GFP localized to junctions in a manner indistinguishable from full-length HMP-1::GFP in a wild-type background,

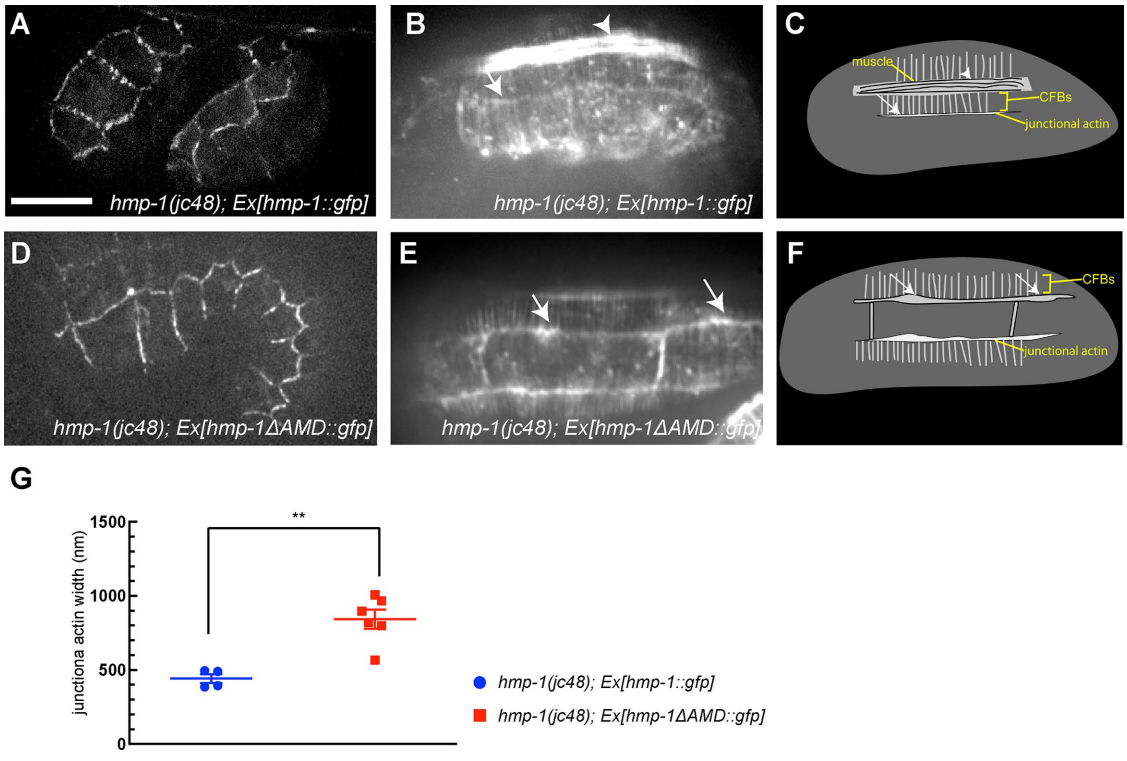

FIGURE 2: HMP-1ΔAMD::GFP recruits more F-actin to junctions. (A) HMP-1::GFP localizes predominantly to adherens junctions in *hmp-1(jc48)* mutants rescued by HMP-1::GFP. Scale bar = 10 μm. (B) Phalloidin staining in *hmp-1(jc48)* mutants rescued by HMP-1::GFP. White arrowhead indicates the underlying muscle. The embryo has parallel circumferential filament bundles (CFBs) and junctional–proximal actin that concentrates along the seam-dorsal boundary (white arrow). (C) Schematics illustrating the actin structures in B. (D) In *hmp-1(jc48)* mutants rescued by HMP-1ΔAMD::GFP and HMP-1ΔAMD::GFP localize to adherens junction, similarly to HMP-1::GFP. (E) Phalloidin staining of *hmp-1(jc48)* mutants rescued by HMP-1ΔAMD::GFP; the arrow points to excessive junctional–proximal actin recruited to junctions by HMP-1ΔAMD::GFP. (F) Schematics of actin structures in E. (G) Quantification of junctional–proximal actin width in *hmp-1(jc48)* mutants rescued by HMP-1::GFP and HMP-1ΔAMD::GFP. Junctional actin is significantly wider in *hmp-1(jc48)* mutants rescued by HMP-1ΔAMD::GFP compared with those rescued by full-length HMP-1::GFP (**, $p \leq 0.01$; Student's *t* test).

indicating that an intact N-terminal HMP-2/β-catenin–binding domain (Shao *et al.*, 2017) is sufficient to target HMP-1ΔAMD::GFP to junctions. HMP-1ΔAMD::GFP rescues *hmp-1(jc48)* mutants, although poorly relative to HMP-1FL::GFP. Embryonic lethality in *hmp-1(jc48);Ex[hmp-1::gfp]* is 52.5%, compared with 88.3% for *hmp-1(jc48);Ex[hmp-1ΔAMD::gfp]*; given that transmission of the extrachromosomal arrays in each case is 52.1 and 53%, respectively, this indicates virtually 100% efficiency of rescue by full-length HMP-1::GFP, but only 23% rescue efficiency in the case of HMP-1ΔAMD::GFP. These results suggest that the AMD is important for the normal function of HMP-1.

To assess how the AMD regulates F-actin recruitment in vivo, we performed phalloidin staining (Figure 2, A–D). The width of the junctional–proximal actin network was significantly greater in *hmp-1(jc48);Ex[hmp-1ΔAMD::gfp]* than in *hmp-1(jc48);Ex[hmp-1::gfp]* embryos (842.4 ± 64.27 nm, $n = 6$ vs. 441.8 ± 29.82 nm, $n = 4$ embryos; significantly different, $p < 0.01$, Student's *t* test). Excessive recruitment of F-actin to adherens junctions by HMP-1ΔAMD::GFP in vivo is consistent with the increased ability of recombinant SUMO::HMP-1ΔAMD to cosediment with F-actin in vitro compared with HMP-1FL.

Unlike HMP-1FL::GFP, which presumably undergoes dynamic, regulated binding to F-actin, the HMP-1ΔAMD::GFP may bind to F-actin in a constitutively active manner, explaining its weak rescue ability. To test this possibility, we introduced an additional mutation (S823F; Maiden *et al.*, 2013) into the HMP-1ΔAMD::GFP construct to slightly reduce its ability to bind F-actin. HMP-1ΔAMD(S823F)::GFP localized to junctions in a manner indistinguishable from HMP-1FL::GFP in a wild-type background (Supplemental Figure S3A). There was only a slight difference in the ability of HMP-1ΔAMD(S823F)::GFP to rescue *hmp-1(jc48)* than HMP-1ΔAMD::GFP (embryonic lethality of *hmp-1(jc48);Ex[hmp-1ΔAMD::gfp]* worms is 88.3%, compared with 78.4% for *hmp-1(jc48);Ex[hmp-1ΔAMD(S823F)::gfp]*; $p < 0.01$, Fisher's exact test), despite ~50% array transmission in each case. However, we found a marked difference in the relative proportions of embryos that died early (Figure 3, A and B). Dead *hmp-1(jc48);Ex[hmp-1ΔAMD::gfp]* embryos tended to die at earlier stages of morphogenesis, with the majority arresting at the 1.5-fold stage or earlier with ruptures; only a small percentage survived beyond the twofold stage. In contrast, the majority of the dead *hmp-1(jc48);Ex[hmp-1ΔAMD(S823F)::gfp]* embryos were able to survive to a later stage, with most arresting at the three- to fourfold stage (Figure 3B). Moreover, less HMP-1ΔAMD(S823F) recombinant protein cosedimented with F-actin in vitro than with HMP-1ΔAMD (Figure 3C and Supplemental Figure S4B). Taken together, these results suggest that deleting the HMP-1 AMD leads to higher binding of F-actin and

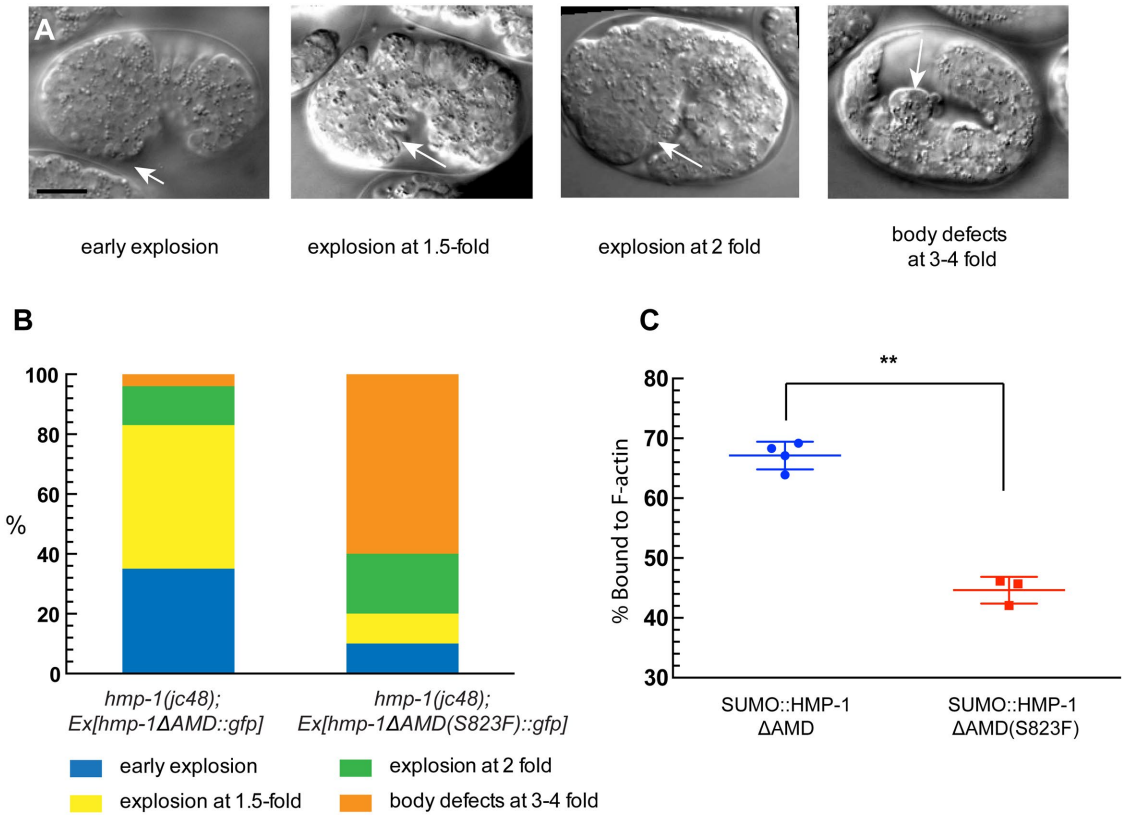

FIGURE 3: The S823F mutation ameliorates the effects of deletion of the HMP-1 AMD. (A) Differential interference contrast (DIC) images of representative embryos used in scoring rescue of morphogenetic defects. Early rupture; the arrow shows extruded anterior cells. Explosion at the 1.5-fold stage; the arrow points to the ruptured anterior region. Head explosion at the twofold stage; the arrow indicates the site of rupture. Arrest at the three- to fourfold stage with body morphology defects; the arrow points to a rupture in the posterior part of the embryo. Scale bar = 10 μm. (B) Scoring of stage of arrest of dead *hmp-1(jc48)* mutants expressing HMP-1ΔAMD::GFP or HMP-1ΔAMD(S823F)::GFP. (C) Quantification of data from actin cosedimentation experiments for SUMO::HMP-1ΔAMD and SUMO::HMP-1ΔAMD(S823F). Error bars represent mean ± SEM ($n = 3$ for HMP-1ΔAMD(S823F) and HMP-1ΔAMD; **, $p \leq 0.05$).

excessive F-actin recruitment at junctions, which can be partially offset by a reduction in the intrinsic binding affinity of the C-terminus for F-actin.

The N-terminus of the HMP-1 ABD is required for full function

Our previous studies (Kwiatkowski *et al.*, 2010; Maiden *et al.*, 2013; Kang *et al.*, 2017) did not assess the importance of the N-terminal portion of the HMP-1 ABD for actin binding. We therefore made a SUMO::HMP-1(704–927) construct, which deletes the N-terminal region of the HMP-1 ABD (aa677–703; Figure 4A). Actin cosedimentation assays indicated that the N-terminally truncated HMP-1 C-terminus (704–927) does not bind F-actin as well as the entire HMP-1 ABD (aa677–927; Figure 4, B and C). The corresponding GFP construct (HMP-1Δ677–703::GFP) localized to junctions in a manner indistinguishable from HMP-1FL::GFP in a wild-type background (Figure 4D), and it rescued the embryonic lethality of *hmp-1(jc48)* mutants (introducing HMP-1Δ677–703::GFP into *hmp-1(jc48)* heterozygotes reduced embryonic lethality among their progeny from 25.3%, identical to the 25% expected for 100% lethality among homozygotes, to 15.1%). However, the rescued *hmp-1(jc48)* homozygotes displayed tail morphology defects (white arrow, Figure 4E) not seen in lines rescued with HMP-1FL::GFP. Moreover, although embryonic lethality was rescued, all *hmp-1(jc48);Ex[hmp-1(Δ677–703)::gfp]* embryos died as L1 or L2 larvae. This result suggests that the N-terminus of the HMP-1 ABD is essential for full function. Owing to lack of rescue, we could not unambiguously identify *hmp-1(jc48);Ex[hmp-1(Δ677–703)::gfp]*

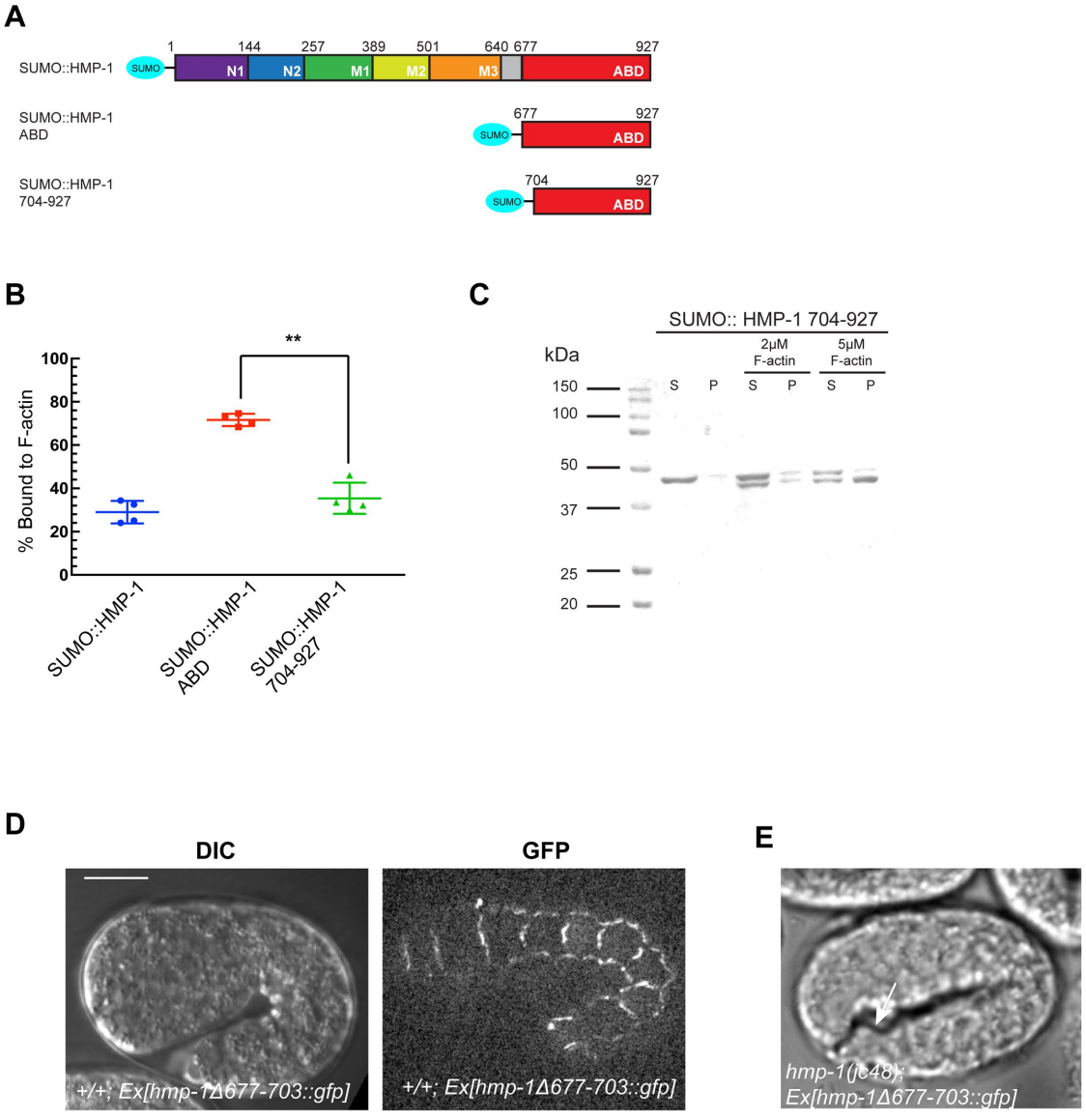

FIGURE 4: The N-terminus of the HMP-1 ABD is important for its proper function during embryonic development. (A) Schematics of the proteins used for actin cosedimentation experiments. (B) Quantification of actin cosedimentation experiments performed using SUMO::HMP-1, SUMO::HMP-1ABD and SUMO::HMP-1 704-927 (**, $p \leq 0.01$; Student's *t* test). (C) Coomassie-stained SDS–PAGE gels of actin cosedimentation experiments using SUMO::HMP-1 704-927 protein constructs at the concentrations indicated. S = supernatant fraction, P = pellet fraction. (D) HMP-1Δ677–703::GFP localizes to adherens junctions in wild-type embryos. Scale bar = 10 μm. (E) *hmp-1(jc48)* mutants rescued by HMP-1Δ677–703::GFP have body morphology defects with a blunt tail (arrow).

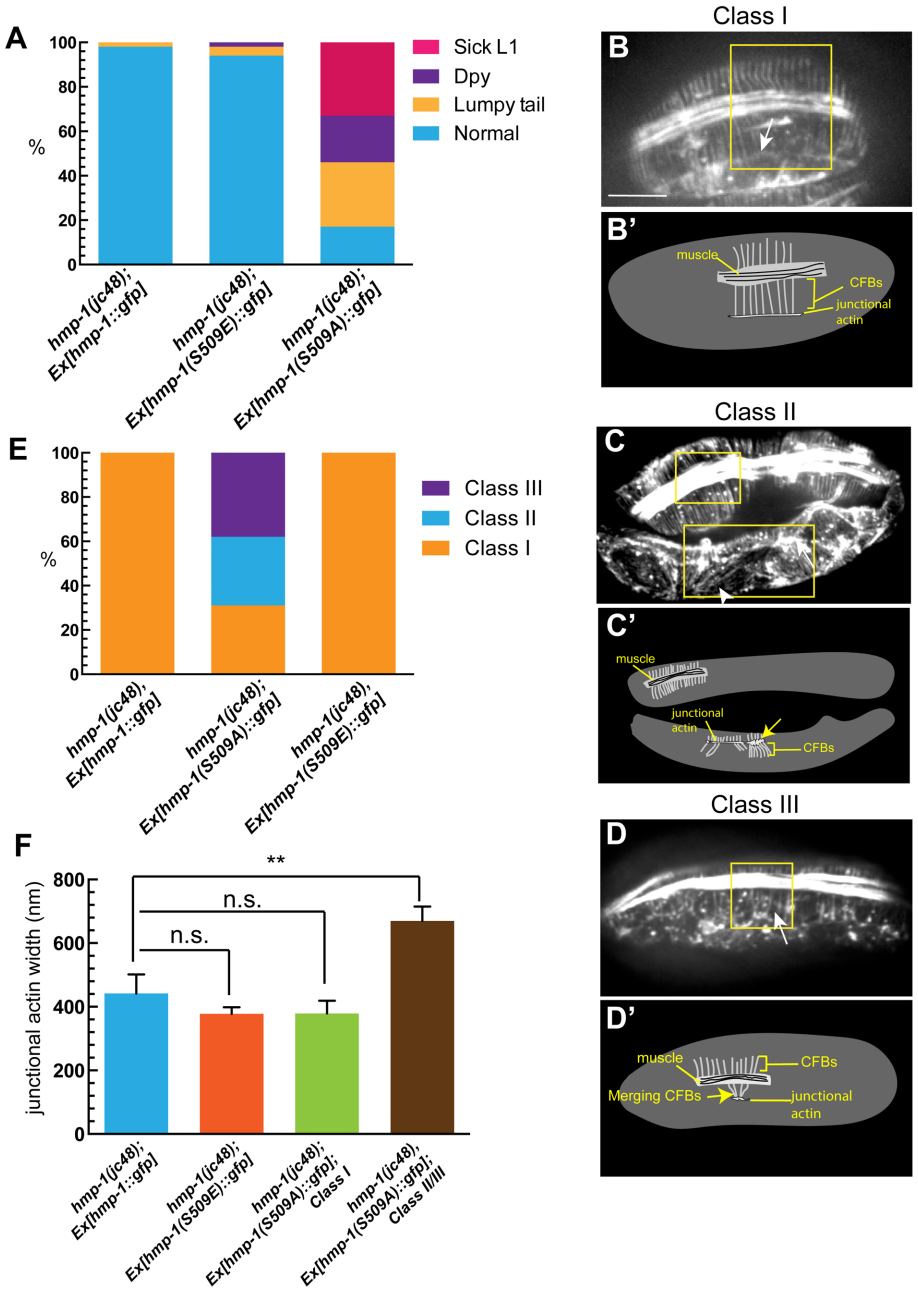

FIGURE 5: Phosphorylation of HMP-1 S509 is important for its normal function. (A) Distribution of the phenotypes of rescued larvae in three different strains: *hmp-1(jc48)* mutants rescued by HMP-1::GFP, HMP-1(S509E)::GFP, and HMP-1(S509A)::GFP. (B–D′) Phalloidin staining (B–D) and schematics of actin structures in the boxed areas (B′–D′). Scale bar = 10 μm. CFB structural defects were grouped into three classes. Class I: normal F-actin organization, parallel, equally spaced CFBs integrated into a network of junctional–proximal actin concentrated along the seam-dorsal boundary; Class II: partially normal F-actin organization with other regions showing irregular organization of CFBs and thick junctional–proximal actin; Class III: multiple CFBs coterminate with thick junctional–proximal actin along the junction. (E) F-actin organization defects in *hmp-1(jc48)* embryos rescued by HMP-1FL::GFP, HMP-1(S509A)::GFP, and HMP-1(S509E)::GFP. (F) Quantification of the width of junctional–proximal actin in *hmp-1(jc48)* embryos rescued by HMP-1FL::GFP, HMP-1(S509A)::GFP, and HMP-1(S509E)::GFP (n.s., not significant; **, $p \leq 0.01$; Student's *t* test).

homozygotes, because processing for phalloidin staining made it difficult to score for the mild tail defects we observed in living larvae; as a result we could not assess subtle defects in junctional–proximal actin in this line.

Phosphorylation of HMP-1 at residue S509 is important for proper function

Phosphorylation and dephosphorylation of the P-linker region (the region between the M and ABD domains) is essential for proper function of *Drosophila* α-catenin (Escobar *et al.*, 2015). However, whether phosphorylation of α-catenin affects its ability to bind F-actin is unclear. We previously found that HMP-1 residues S312, S509, S649, and S910 are subject to phosphorylation (Callaci *et al.*, 2015). S509 and S649 lie within the AMD, so we examined them in more detail by introducing non-phosphorylatable and phosphomimetic mutations into our HMP-1FL::GFP construct. Both HMP-1(S509A)::GFP and HMP-1(S509E)::GFP localize normally to junctions in wild type and were indistinguishable from HMP-1FL::GFP (Supplemental Figure S3, C–F). Both HMP-1(S509A)::GFP and HMP-1(S509E)::GFP rescued the embryonic lethality of *hmp-1(jc48)* mutants; however, L1 offspring of *hmp-1(jc48);Ex[hmp-1(S509A)::gfp]* worms exhibited morphological defects, including Dumpy larvae, Sick L1s, and Lumpy tails (Supplemental Figure S3, G–K). In contrast, progeny of *hmp-1(jc48);Ex[hmp-1(S509E)::gfp]* worms appeared indistinguishable from *hmp-1(jc48)* animals rescued by HMP-1FL::GFP (Figure 5A). These results suggest that phosphorylation of HMP-1 S509 is important for normal function.

We next investigated whether disrupting phosphorylation at S509 affects F-actin recruitment to junctions. Phalloidin staining of *hmp-1(jc48);Ex[hmp-1(S509E)::gfp]* embryos revealed that circumferential actin filament bundles (CFBs) are indistinguishable from those in *hmp-1(jc48);Ex[hmp-1::gfp]* embryos (Figure 5E). In contrast, CFBs in *hmp-1(jc48);Ex[hmp-1(S509A)::gfp]* embryos exhibited a range of CFB morphologies, from normal (Class I; Figure 5, B and B′) to partially irregular (Class II; Figure 5, C and C′) to merging of CFBs at seam-ventral junctions (Class III; Figure 5, D and D′). Quantification of junctional–proximal actin width in *hmp-1(jc48);Ex[hmp-1(S509A)::gfp]* embryos showed that in embryos with normal CFBs the width of the junctional–proximal actin array did not differ significantly from *hmp-1(jc48);Ex[hmp-1(S509E)::gfp]* or *hmp-1(jc48);Ex[hmp-1::gfp]* embryos (Figure 5F). However, in *hmp-1(jc48);Ex[hmp-1(S509A)::gfp]* embryos exhibiting Class II and Class III defects, the width of junctional–proximal actin was significantly greater than in *hmp-1(jc48);Ex[hmp-1(S509E)::gfp]* or *hmp-1(jc48);Ex[hmp-1::gfp]* embryos (Figure 5F), suggesting that the abnormal CFB organization

in *hmp-1(jc48);Ex[hmp-1(S509A)::gfp]* embryos may be due to excessive actin recruited to junctions.

In contrast to the effects upon mutating S509, both HMP-1(S649E)::GFP and HMP-1(S649A)::GFP localized correctly to junctions, with HMP-1(S649E)::GFP showing more cytoplasmic signal (Supplemental Figure S4, A and B). Although both HMP-1(S649A)::GFP and HMP-1(S649E)::GFP rescued *hmp-1(jc48)* embryonic lethality, HMP-1(S649A)::GFP rescued more efficiently than HMP-1(S649E)::GFP (56.4% embryonic lethality for *hmp-1(jc48);Ex[hmp-1(S649A)::gfp]* worms vs. 69.3% embryonic lethality for *hmp-1(jc48);Ex[hmp-1(S649E)::gfp]* worms, respectively). Phalloidin staining indicated that CFBs and junctional–proximal actin were normal in both strains (Supplemental Figure S4, C and D), with no difference from mutants rescued with unmutated HMP-1FL::GFP (Supplemental Figure S4E). Thus the phosphorylation status of HMP-1 S649 has only subtle effects on proper HMP-1 function during embryogenesis compared with S509.

Conclusion: The HMP-1 AMD negatively regulates F-actin binding

Although the AMD of α-catenin has been suggested to be a regulator of α-catenin function (Imamura *et al.*, 1999), the in vivo significance of the AMD has remained unclear for nearly two decades. Our results suggest that the HMP-1 AMD negatively regulates F-actin binding, because *hmp-1(jc48);Ex[hmp-1ΔAMD::gfp]* embryos possess excessive F-actin at junctions compared with wild type. Actin cosedimentation assays further suggest that recruitment of excess F-actin is due to excessive binding of HMP-1ΔAMD to F-actin. Excessive binding to F-actin may be deleterious during dynamic morphogenetic movements; at such times, the organization and assembly of the F-actin cytoskeleton must presumably be labile enough to accommodate dramatic changes in the shape and position of cells during epithelial morphogenesis. Adding a point mutation within the C-terminus of HMP-1ΔAMD::GFP known to weaken binding to F-actin (Maiden *et al.*, 2013) supports the idea that the AMD normally maintains the affinity of HMP-1 for F-actin within an optimal functional range, because the mutated HMP-1ΔAMD::GFP functions better in a rescue assay.

Our results suggest a model for negative regulation of HMP-1 binding to F-actin via its AMD that involves multiple mechanisms (Supplemental Figure S5). One potential regulator is tension; either tension applied to HMP-1 or tension applied to the F-actin networks to which HMP-1 attaches. Recent research has shown that the affinity of the cadherin–β-catenin–αE-catenin ternary complex for F-actin increases dramatically when tension is applied to the actin (Buckley *et al.*, 2014). Future experiments aimed at determining whether HMP-1 exhibits a tension-mediated increase in binding affinity for F-actin, and the role the AMD plays in this response, would prove extremely interesting.

Second, the AMD may be regulated through phosphorylation. That *hmp-1(jc48)* mutants rescued by a nonphosphorylatable mutant form of HMP-1::GFP (HMP-1(S509A)::GFP) exhibited more morphological defects compared with those rescued by an S509 phosphomimetic mutant suggests that HMP-1 phosphorylation at S509 is important for its proper function. Dephosphorylation of S509 may lead to excessive binding of HMP-1 to F-actin. That *hmp-1(jc48);Ex[hmp-1(S509A)::gfp]* embryos display abnormalities in F-actin organization is consistent with this possibility. Phosphoregulation of S641 in mammalian αE-catenin and the corresponding T645 in *Drosophila* α-catenin appears to be required for normal function (Escobar *et al.*, 2015). Our results suggest that phosphoregulation of the corresponding residue in HMP-1, S649, plays a relatively minor role.

Finally, although not shown in Supplemental Figure S5, the HMP-1 AMD could regulate binding to other partners. The most heavily studied M domain binding partner of vertebrate αE-catenin is vinculin (Yonemura *et al.*, 2010; Choi *et al.*, 2012; Rangarajan and Izard, 2012; Ishiyama *et al.*, 2013; Thomas *et al.*, 2013). Even though the M1 domain of HMP-1 can bind vertebrate vinculin avidly, its binding to DEB-1, the *C. elegans* vinculin homologue, is very weak (Kang *et al.*, 2017), and DEB-1 is not expressed in the epidermis in *C. elegans* (Barstead and Waterston, 1989). Although HMP-1 appears to have lost the ability to associate with *C. elegans* vinculin, other binding partners may associate with HMP-1 via unfurling of its M domain.

In addition to our analysis of the AMD, we identified aa677–704 of HMP-1 as necessary for F-actin binding. While this work was under review, a role for the α1 helix of the ABD (aa669–675 of αE-catenin, corresponding to aa676–681 of HMP-1) in negatively regulating the binding of α-catenin to F-actin was identified (Ishiyama *et al.*, 2018). In that study deletion of α1 led to increased binding to F-actin, similar to our AMD deletions. Our larger N-terminal ABD deletion includes α1, α2, and part of the α3 domains of the ABD, which likely accounts for the difference in results from Ishiyama *et al*. Thus there may be several conformation-dependent regulatory domains within α-catenins that regulate their binding to F-actin, including the AMD and α1 within the ABD.

MATERIALS AND METHODS

Nematode strains and genetics

C. elegans strains were maintained using standard methods (Brenner, 1974). Bristol N2 was used as wild type. The following allele was utilized in this study*: hmp-1(jc48)*. The following transgenic arrays were made for or used in this study: *hmp-1::gfp*, *hmp-1Δ504–676::gfp*, *hmp-1Δ504–676+S823F::gfp*, *hmp-1Δ677–703::gfp*, each under its endogenous promoter.

Standard genetic crosses were used to create *hmp-1(jc48);Ex[HMP-1::GFP]* homozygotes, along with the introduction of other *hmp-1* rescuing constructs.

Strains were made by DNA microinjection: 1 ng/µl of the transgene of interest, in addition to 20 ng/µl noncoding DNA (F35D3) and 79 ng/µl *rol-6(su1006)*, was injected into the gonads of N2, as described previously (Mello and Fire, 1995). Comparable expression of all transgenes was confirmed using methods described previously (Shao *et al.*, 2017).

CRISPR

The *hmp-1(jc48)* null mutant allele was generated via CRISPR following a protocol described previously (Arribere *et al.*, 2014). Primer XS77: 5′ TGC CTG CGA AGT TTT AGA GCT AGA AAT AGC 3′ and primer XS78(REV): 5′ TTC TGA AAA CAA GAC ATC TCG CAA TAG GA 3′ were used for making sgRNA constructs. The single-stranded DNA repair template (5′ TATTTCTCTTCGTTTTATTTGCATTCTAATC TGAATTTTCAATTTTATTAATTTTCAGAATGCCTTAAAATAACAATT CTCATGCGTATTTCAACATCGACGAAGTGCGCTCGAAAAATG 3′) was synthesized by Integrated DNA Technologies (Coralville, IA).

Imaging

Embryos were isolated from gravid hermaphrodites, mounted on a 5% agarose pad, and aged at 20–25°C until the onset of morphogenesis. For four-dimensional differential interference contrast microscopy, embryos were imaged using 1-µm slice spacing at 3-min intervals using a Nikon Optiphot 2 microscope with a 60×/1.4 NA oiled objective at 20°C with a Macintosh computer running ImageJ (https://imagej.nih.gov/ij/; Schneider *et al.*, 2012) using custom

macros/plug-ins (available at worms.zoology.wisc.edu/research/4d/4d.html). For fluorescent imaging, a Perkin-Elmer UltraView spinning disk confocal microscope, mounted on a Nikon Eclipse E600 microscope, equipped with a Hamamatsu ORCA-ER camera and controlled by Micro-Manager software (https://micromanager.org/; Edelstein *et al.*, 2014), was used to collect images of GFP expressing embryos, using 0.5-µm slices at 3-min intervals with a 60×/1.4 NA oil objective at 20°C. Antibody staining (0.6-µm slices) and phalloidin staining (0.2-µm slices) images were collected with the same confocal microscope using a 100×/1.45 NA total internal reflection fluorescence objective.

Protein expression and purification

SUMO-His-tagged proteins were expressed in BL21-Gold(DE3) *Escherichia coli* cells and purified as described (Mayers *et al.*, 2011; Maiden *et al.*, 2013). Cells were induced with 0.1 mM isopropyl β-D-1 thiogalactopyranoside at 18°C for 16 h. Wash and elution buffers were as follows: His wash (50 mM Na-phosphate, pH 8.0, 300 mM NaCl, 0.1% Tween-20, 10 mM imidazole), and His elution (250 mM imidazole, 100 mM NaCl, 10% glycerol, 50 mM HEPES, pH 7.6).

Actin-pelleting assays

Actin-pelleting assays were performed as described previously (Maiden *et al.*, 2013). Briefly, 5 µM purified proteins (quantified via a Bradford assay; Pierce/Thermo Scientific) was incubated at room temperature for 1 h with 0, 2, or 5 µM polymerized chicken F-actin (Cytoskeleton, Denver, CO). Samples were then centrifuged at 100,000 rpm for 20 min at 4°C in a TLA-100 rotor in a tabletop ultracentrifuge (Beckman Optima TL 100 Ultracentrifuge). Samples were run on 12% SDS–PAGE gels and stained with Coomassie Brilliant Blue, and bands were quantified using ImageJ software. To determine the percentage of protein bound to F-actin, background sedimentation of the protein (no actin control) was subtracted first and each band intensity was then normalized to the pelleted F-actin.

Antibody and phalloidin staining

Freeze-cracking was used for immunostaining embryos (Albertson, 1984). Staining was performed as described previously (Leung *et al.*, 1999). Embryos were incubated with primary antibodies in phosphate-buffered saline + 0.1% Tween-20 (PBST) and 1% nonfat dry milk overnight at 4°C. Embryos were then incubated with secondary antibodies in PBST and 1% nonfat dry milk for 4 h at room temperature. The following primary antibodies were used: 1:1000 mouse-anti-GFP (Invitrogen), 1:4000 polyclonal rabbit-anti-HMP-1 (Zaidel-Bar *et al.*, 2010), and 1:200 mouse monoclonal anti-AJM-1 (MH27; Francis and Waterston, 1991). The following secondary antibodies were used: 1:50 anti-rabbit immunoglobulin G Texas Red, 1:50 anti-rabbit Cy5, and 1:50 anti-mouse fluorescein isothiocyanate.

Phalloidin staining of mutant and wild-type embryos was used to visualize F-actin in fixed embryos (Costa *et al.*, 1998). Embryos were fixed using the following: 4% paraformaldehyde, 0.1 mg/ml lysolecithin, 48 mM PIPES, pH 6.8, 25 mM HEPES, pH 6.8, 2 mM $MgCl_2$, and 10 mM EGTA (ethylene glycol-bis(β-aminoethyl ether)-*N*,*N*,*N*′,*N*′-tetraacetic acid) for 20 min at room temperature. Phalloidin-Texas Red (1:20; Thermo Fisher) was incubated with embryos overnight at 4°C. Quantification of junctional actin width was performed using a single-blind approach from unidentified stained specimens in ImageJ using a microscope stage micrometer as a reference for normalizing scale.

ACKNOWLEDGMENTS

We thank Tim Loveless for helpful discussions regarding experiments and manuscript preparation and Bill Weis for comments on the manuscript. This project was funded by Grant no. GM-058038 from the National Institutes of Health and Grant no. 60698 from the John Templeton Foundation to J.H.

REFERENCES

Albertson DG (1984). Formation of the first cleavage spindle in nematode embryos. Dev Biol 101, 61–72.

Arribere JA, Bell RT, Fu BX, Artiles KL, Hartman PS, Fire AZ (2014). Efficient marker-free recovery of custom genetic modifications with CRISPR/Cas9 in *Caenorhabditis elegans*. Genetics 198, 837–846.

Barstead RJ, Waterston RH (1989). The basal component of the nematode dense-body is vinculin. J Biol Chem 264, 10177–10185.

Brenner S (1974). The genetics of *Caenorhabditis elegans*. Genetics 77, 71–94.

Buckley CD, Tan J, Anderson KL, Hanein D, Volkmann N, Weis WI, Nelson WJ, Dunn AR (2014). Cell adhesion. The minimal cadherin-catenin complex binds to actin filaments under force. Science 346, 1254211.

Callaci S, Morrison K, Shao X, Schuh AL, Wang Y, Yates JR 3rd, Hardin J, Audhya A (2015). Phosphoregulation of the *C. elegans* cadherin-catenin complex. Biochem J 472, 339–352.

Choi HJ, Pokutta S, Cadwell GW, Bobkov AA, Bankston LA, Liddington RC, Weis WI (2012). αE-catenin is an autoinhibited molecule that coactivates vinculin. Proc Natl Acad Sci USA 109, 8576–8581.

Costa M, Raich W, Agbunag C, Leung B, Hardin J, Priess JR (1998). A putative catenin-cadherin system mediates morphogenesis of the *Caenorhabditis elegans* embryo. J Cell Biol 141, 297–308.

Desai R, Sarpal R, Ishiyama N, Pellikka M, Ikura M, Tepass U (2013). Monomeric α-catenin links cadherin to the actin cytoskeleton. Nat Cell Biol 15, 261–273.

Drees F, Pokutta S, Yamada S, Nelson WJ, Weis WI (2005). α-Catenin is a molecular switch that binds E-cadherin-β-catenin and regulates actin-filament assembly. Cell 123, 903–915.

Edelstein AD, Tsuchida MA, Amodaj N, Pinkard H, Vale RD, Stuurman N (2014). Advanced methods of microscope control using μManager software. J Biol Methods 1, e10.

Escobar DJ, Desai R, Ishiyama N, Folmsbee SS, Novak MN, Flozak AS, Daugherty RL, Mo R, Nanavati D, Sarpal R, *et al.* (2015). α-Catenin phosphorylation promotes intercellular adhesion through a dual-kinase mechanism. J Cell Sci 128, 1150–1165.

Francis R, Waterston RH (1991). Muscle cell attachment in *Caenorhabditis elegans*. J Cell Biol 114, 465–479.

Harris TJ, Tepass U (2010). Adherens junctions: from molecules to morphogenesis. Nat Rev Mol Cell Biol 11, 502–514.

Herrenknecht K, Ozawa M, Eckerskorn C, Lottspeich F, Lenter M, Kemler R (1991). The uvomorulin-anchorage protein alpha catenin is a vinculin homologue. Proc Natl Acad Sci USA 88, 9156–9160.

Huveneers S, Oldenburg J, Spanjaard E, van der Krogt G, Grigoriev I, Akhmanova A, Rehmann H, de Rooij J (2012). Vinculin associates with endothelial VE-cadherin junctions to control force-dependent remodeling. J Cell Biol 196, 641–652.

Imamura Y, Itoh M, Maeno Y, Tsukita S, Nagafuchi A (1999). Functional domains of α-catenin required for the strong state of cadherin-based cell adhesion. J Cell Biol 144, 1311–1322.

Ishiyama N, Sarpal R, Wood MN, Barrick SK, Nishikawa T, Hayashi H, Kobb AB, Flozak AS, Yemelyanov A, Fernandez-Gonzalez R, *et al.* (2018). Force-dependent allostery of the α-catenin actin-binding domain controls adherens junction dynamics and functions. Nat Commun 9, 5121.

Ishiyama N, Tanaka N, Abe K, Yang YJ, Abbas YM, Umitsu M, Nagar B, Bueler SA, Rubinstein JL, Takeichi M, Ikura M (2013). An autoinhibited structure of α-catenin and its implications for vinculin recruitment to adherens junctions. J Biol Chem 288, 15913–15925.

Kang H, Bang I, Jin KS, Lee B, Lee J, Shao X, Heier JA, Kwiatkowski AV, Nelson WJ, Hardin J, *et al.* (2017). Structural and functional characterization of *Caenorhabditis elegans* α-catenin reveals constitutive binding to β-catenin and F-actin. J Biol Chem 292, 7077–7086.

Kwiatkowski AV, Maiden SL, Pokutta S, Choi HJ, Benjamin JM, Lynch AM, Nelson WJ, Weis WI, Hardin J (2010). In vitro and in vivo reconstitution of the cadherin–catenin–actin complex from *Caenorhabditis elegans*. Proc Natl Acad Sci USA 107, 14591–14596.

Leung B, Hermann GJ, Priess JR (1999). Organogenesis of the *Caenorhabditis elegans* intestine. Dev Biol 216, 114–134.
Maiden SL, Harrison N, Keegan J, Cain B, Lynch AM, Pettitt J, Hardin J (2013). Specific conserved C-terminal amino acids of *Caenorhabditis elegans* HMP-1/α-catenin modulate F-actin binding independently of vinculin. J Biol Chem 288, 5694–5706.
Mandai K, Nakanishi H, Satoh A, Obaishi H, Wada M, Nishioka H, Itoh M, Mizoguchi A, Aoki T, Fujimoto T, *et al*. (1997). Afadin: A novel actin filament-binding protein with one PDZ domain localized at cadherin-based cell-to-cell adherens junction. J Cell Biol 139, 517–528.
Mayers JR, Fyfe I, Schuh AL, Chapman ER, Edwardson JM, Audhya A (2011). ESCRT-0 assembles as a heterotetrameric complex on membranes and binds multiple ubiquitinylated cargoes simultaneously. J Biol Chem 286, 9636–9645.
Mello C, Fire A (1995). DNA transformation. In: Caenorhabditis elegans: Modern Biologcial Analysis of an Organism, Amsterdam: Elsevier BV, 451–482.
Ozawa M, Baribault H, Kemler R (1989). The cytoplasmic domain of the cell adhesion molecule uvomorulin associates with three independent proteins structurally related in different species. EMBO J 8, 1711–1717.
Pettitt J, Cox EA, Broadbent ID, Flett A, Hardin J (2003). The *Caenorhabditis elegans* p120 catenin homologue, JAC-1, modulates cadherin-catenin function during epidermal morphogenesis. J Cell Biol 162, 15–22.
Pokutta S, Choi HJ, Ahlsen G, Hansen SD, Weis WI (2014). Structural and thermodynamic characterization of cadherin·β-catenin·α-catenin complex formation. J Biol Chem 289, 13589–13601.
Pokutta S, Drees F, Takai Y, Nelson WJ, Weis WI (2002). Biochemical and structural definition of the l-afadin- and actin-binding sites of α-catenin. J Biol Chem 277, 18868–18874.
Pokutta S, Weis WI (2000). Structure of the dimerization and β-catenin-binding region of α-catenin. Mol Cell 5, 533–543.
Rangarajan ES, Izard T (2012). The cytoskeletal protein α-catenin unfurls upon binding to vinculin. J Biol Chem 287, 18492–18499.
Rangarajan ES, Izard T (2013). Dimer asymmetry defines α-catenin interactions. Nat Struct Mol Biol 20, 188–193.
Schneider CA, Rasband WS, Eliceiri KW (2012). NIH Image to ImageJ: 25 years of image analysis. Nat Methods 9, 671–675.
Shao X, Kang H, Loveless T, Lee GR, Seok C, Weis WI, Choi HJ, Hardin J (2017). Cell-cell adhesion in metazoans relies on evolutionarily conserved features of the α-catenin·β-catenin-binding interface. J Biol Chem 292, 16477–16490.
Takeichi M (2014). Dynamic contacts: rearranging adherens junctions to drive epithelial remodelling. Nat Rev Mol Cell Biol 15, 397–410.
Thomas WA, Boscher C, Chu YS, Cuvelier D, Martinez-Rico C, Seddiki R, Heysch J, Ladoux B, Thiery JP, Mege RM, Dufour S (2013). α-Catenin and vinculin cooperate to promote high E-cadherin-based adhesion strength. J Biol Chem 288, 4957–4969.
Watabe-Uchida M, Uchida N, Imamura Y, Nagafuchi A, Fujimoto K, Uemura T, Vermeulen S, van Roy F, Adamson ED, Takeichi M (1998). α-Catenin-vinculin interaction functions to organize the apical junctional complex in epithelial cells. J Cell Biol 142, 847–857.
Yonemura S, Wada Y, Watanabe T, Nagafuchi A, Shibata M (2010). alpha-Catenin as a tension transducer that induces adherens junction development. Nat Cell Biol 12, 533–542.
Zaidel-Bar R, Joyce MJ, Lynch AM, Witte K, Audhya A, Hardin J (2010). The F-BAR domain of SRGP-1 facilitates cell–cell adhesion during *C. elegans* morphogenesis. J Cell Biol 191, 761–769.

Supplemental Materials

Molecular Biology of the Cell

Shao et al.

Supplemental Materials

Figure S1*.hmp-1(jc48) *mutants show classic Hmp phenotypes.(A) A schematic representation of the *hmp-1(jc48)* lesion. *hmp-1(jc48)* mutates Serine 3 to a stop codon. (B) DIC and confocal images of a typical *hmp-1(jc48)* mutant embryo. Anterior is left, dorsal is up. Scale bar is 10 µm. *hmp-1(jc48)* homozygotesarrest during embryonic elongation with the characteristic dorsal epidermal folds previously described in *hmp-1* mutants(Costa *et al.*, 1998; Maiden *et al.*, 2013). A dorsal fold has formed in the epidermis (arrow) at the elongation stage as the embryo reflexes dorsally, indicative of loss of function of HMP-1. (C-E) Double antibody staining of *hmp-1(jc48)* mutant embryos. Anterior is left, posterior is right. Anti-HMP-1 in red; anti-AJM-1 in green, marking cell-cell contacts. No HMP-1 protein was detectable via immunostaining in dead embryos (Fig. S1C-S1E), indicating that*hmp-1(jc48)* is a true protein null allele.(F-G) Staining with fluorophore-conjugated phalloidin in a wild-type(WT) (F) and *hmp-1(jc48)* mutant embryo (G) to visualize F-actin organization. In the wild-type embryo in (F), parallel CFBs are prominent; white arrowhead indicates the underlying muscle. In contrast, in the *hmp-1(jc48)* mutant embryo in (G), large gaps between CFBs are evident, as well as thicker bundles of CFBs (red arrow); this embryo also lacks junctional proximal actin in the epidermis, as evidence by gaps in phalloidin signal at the seam-dorsal boundary (green arrow). Scale bar = 10 µm.

Figure S2: Quantification of in vivo expression level of hmp-1::gfp and related variants. Quantification of *hmp-1::gfp, hmp-1ΔAMD::gfp, hmp-1ΔAMD(S823F)::gfp, hmp-1Δ677-703::gfp, hmp-1S509A::gfp; hmp-1S509E::gfp; hmp-1S649A::gfp, hmp-*

1S649E::gfp revealed no significant difference in expression level. (p=0.3139, one-way ANOVA). Z-projections of 8 focal planes were measured for each junction.

Figure S3.Effects of point mutations on HMP-1 function. (A) HMP-1ΔAMD(S823F)::GFP localizes correctly to junctions in an elongating embryo. Scale bar = 10 µm. (B) Coomassie-stained SDS-PAGE gels of actin cosedimentation experiments using SUMO::HMP-1ΔAMD protein constructs at the concentrations indicated. S = supernatant fraction, P = pellet fraction. (C-D) DIC and confocal images of a wild-type embryo expressing HMP-1(S509A)::GFP, which localizes to cell-cell junctions. Scale bar is 10 µm. (E-F) DIC and confocal images of a wild-type embryo expressing HMP-1(S509E)::GFP, which likewise localizes to cell-cell junctions. (G-K) DIC images illustrating representative body morphology defects in L1 offspring of *hmp-1(jc48);Ex[hmp-1(S509A)::gfp]* worms.(G) Wildtype; (H) Dpy/Dumpy larva; (I) larva with Lumpy tail;(J) Sick L1:larvawith disorganized bulges (arrow) within different regions of the body. Scale bar = 20µm.

Figure S4. Phosphorylation of HMP-1 at S649 does not have a significant role in regulating F-actin organization during embryonic development.(A-B) Spinning disc confocal microscopy shows that both HMP-1(S649A)::GFP and HMP-1(S649E)::GFP localize to cell-cell junctions. Note that a higher percentage of HMP-1(S649E)::GFP is in the cytoplasm compared with HMP-1(S649A)::GFP. Scale bar =10 µm.(C-D) Staining with fluorophore-conjugated phalloidin in a *hmp-1(jc48)* mutant embryos rescued by HMP-1(S649A)::GFP (C) and HMP-1(S649E)::GFP (D) to visualize the F-actin organization. F-actin organization in both embryos appears indistinguishable from

wildtype, with parallel CFBs. In both figures, white arrowheads indicate the underlying muscle and white arrow points to junctional-proximal actin that concentrates along the junction.(E) Quantification of the width of junctional-proximal actin in the embryos of *hmp-1(jc48)* mutants rescued by HMP-1::GFP, HMP-1(S649A)::GFP and HMP-1(S649E)::GFP. (n.s., not significant; Student's T-test).

Figure S5. A model for AMD function in regulation of HMP-1 binding to F-actin. HMP-1 binds weakly to F-actin in its autoinhibited state, which is conferred in part through the conformation of the AMD. When autoinhibition is relieved, possibly through dephosphorylation of HMP-1 S509 or via tension, the activated C terminus of HMP-1 binds F-actin more readily (red star), leading to increased recruitment of F-actin to adherens junctions.

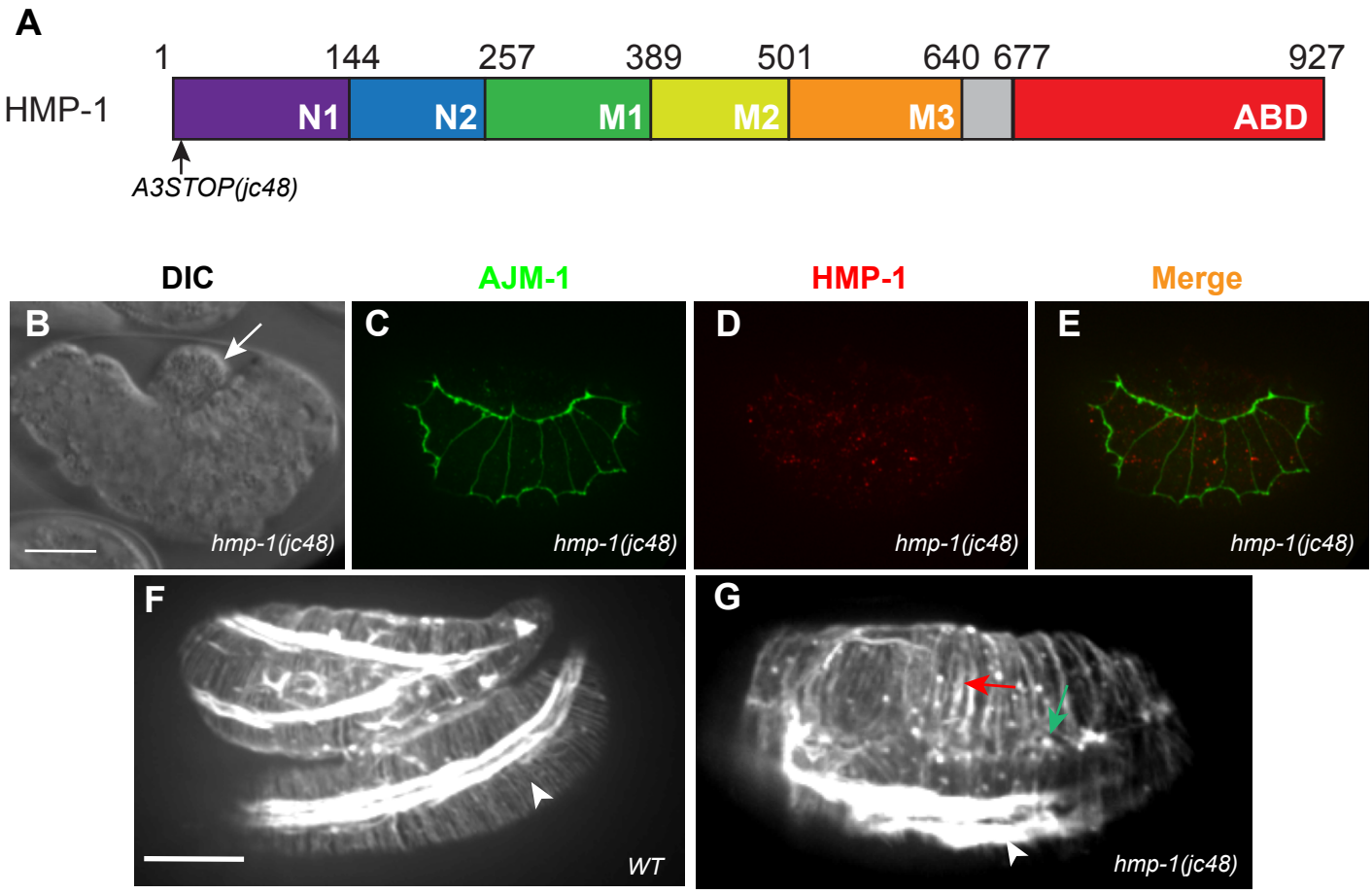
A
1
144
257
389
501
640
677
927
HMP-1
N1
N2
M1
M2
M3
ABD
A3STOP(jc48)
DIC
AJM-1
HMP-1
Merge
B
C
D
E
hmp-1(jc48)
hmp-1(jc48)
hmp-1(jc48)
hmp-1(jc48)
F
G
WT
hmp-1(jc48)

Figure S1

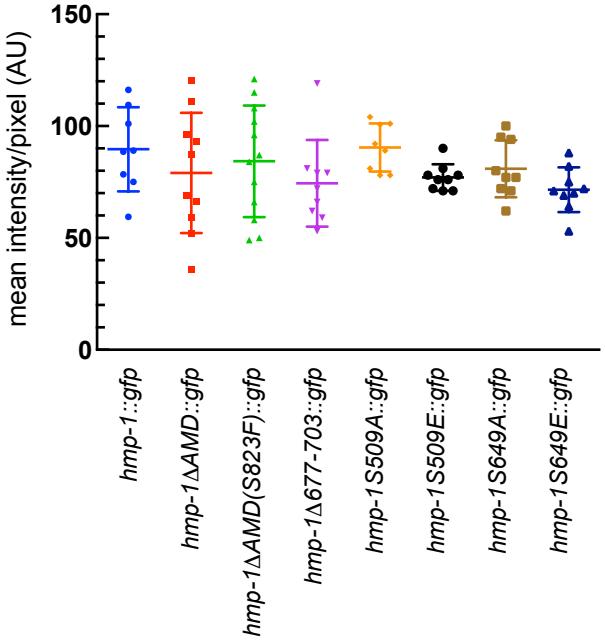
mean intensity/pixel (AU)
150
100
50
0
hmp-1::gfp
hmp-1ΔAMD::gfp
hmp-1ΔAMD(S823F)::gfp
hmp-1Δ677-703::gfp
hmp-1S509A::gfp
hmp-1S509E::gfp
hmp-1S649A::gfp
hmp-1S649E::gfp

Figure S2

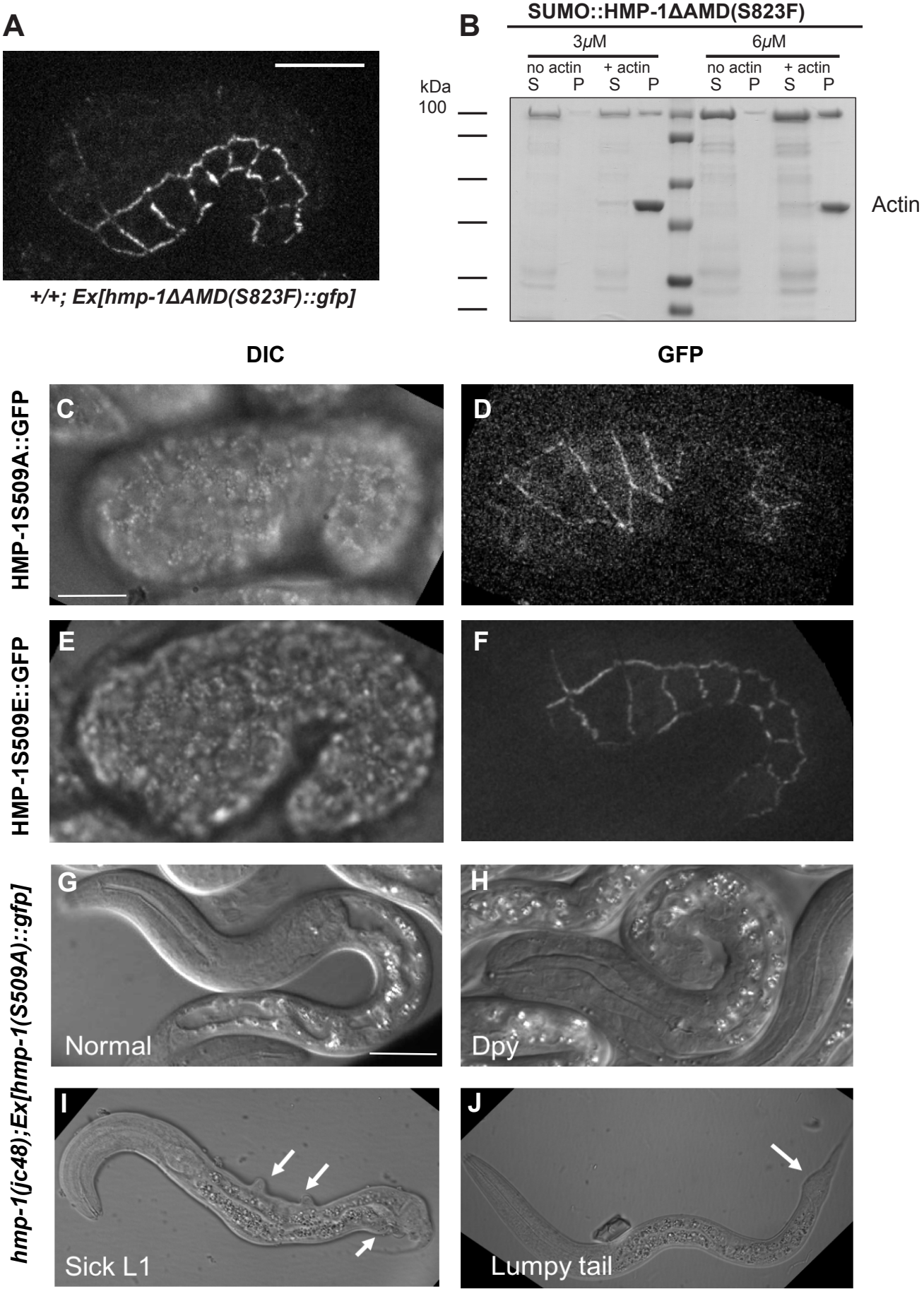
A
+/+; Ex[hmp-1ΔAMD(S823F)::gfp]
B
SUMO::HMP-1ΔAMD(S823F)
3μM
6μM
no actin
+ actin
no actin
+ actin
S P S P S P S P
kDa
100
Actin
DIC
GFP
HMP-1S509A::GFP
C
D
HMP-1S509E::GFP
E
F
hmp-1(jc48);Ex[hmp-1(S509A)::gfp]
G
Normal
H
Dpy
I
Sick L1
J
Lumpy tail

Figure S3

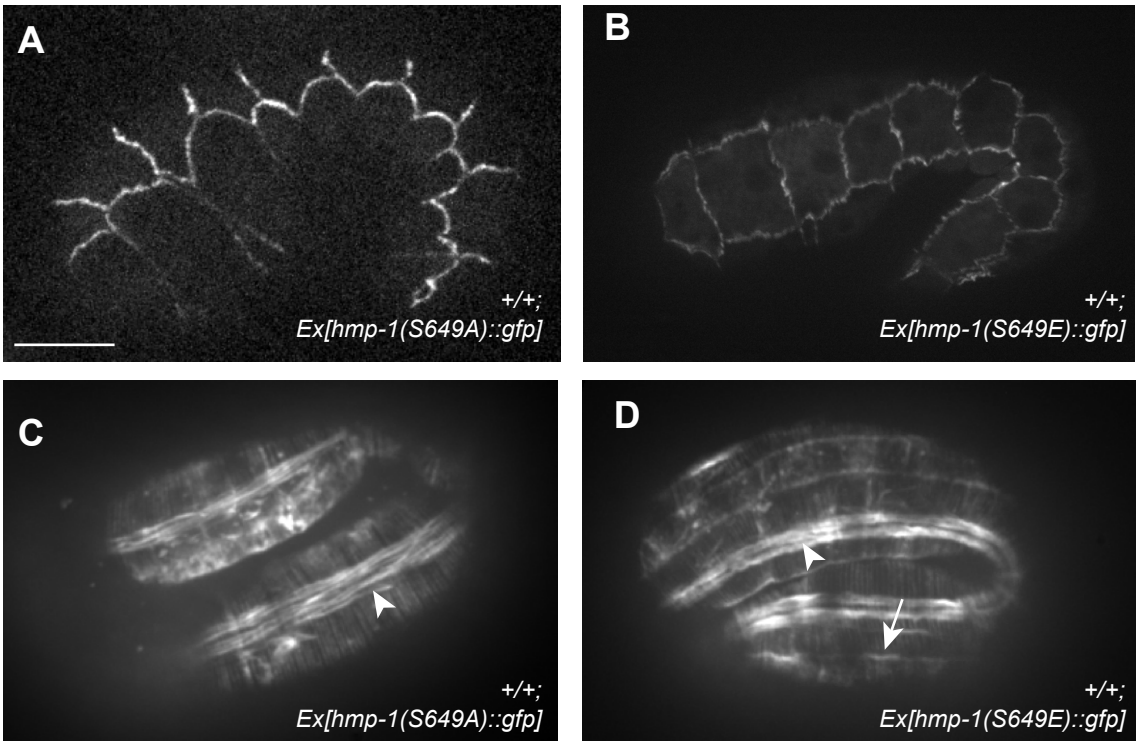
A
+/+;
Ex[hmp-1(S649A)::gfp]
B
+/+;
Ex[hmp-1(S649E)::gfp]
C
+/+;
Ex[hmp-1(S649A)::gfp]
D
+/+;
Ex[hmp-1(S649E)::gfp]

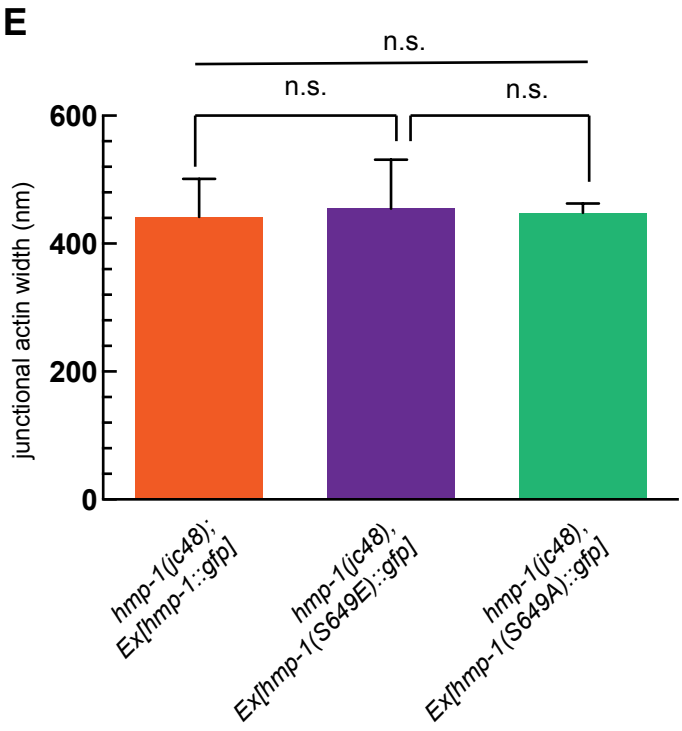
E
n.s.
n.s.
n.s.
600
400
200
0
junctional actin width (nm)
hmp-1(ic48);
Ex[hmp-1::gfp]
hmp-1(ic48);
Ex[hmp-1(S649E)::gfp]
hmp-1(ic48);
Ex[hmp-1(S649A)::gfp]

Figure S4

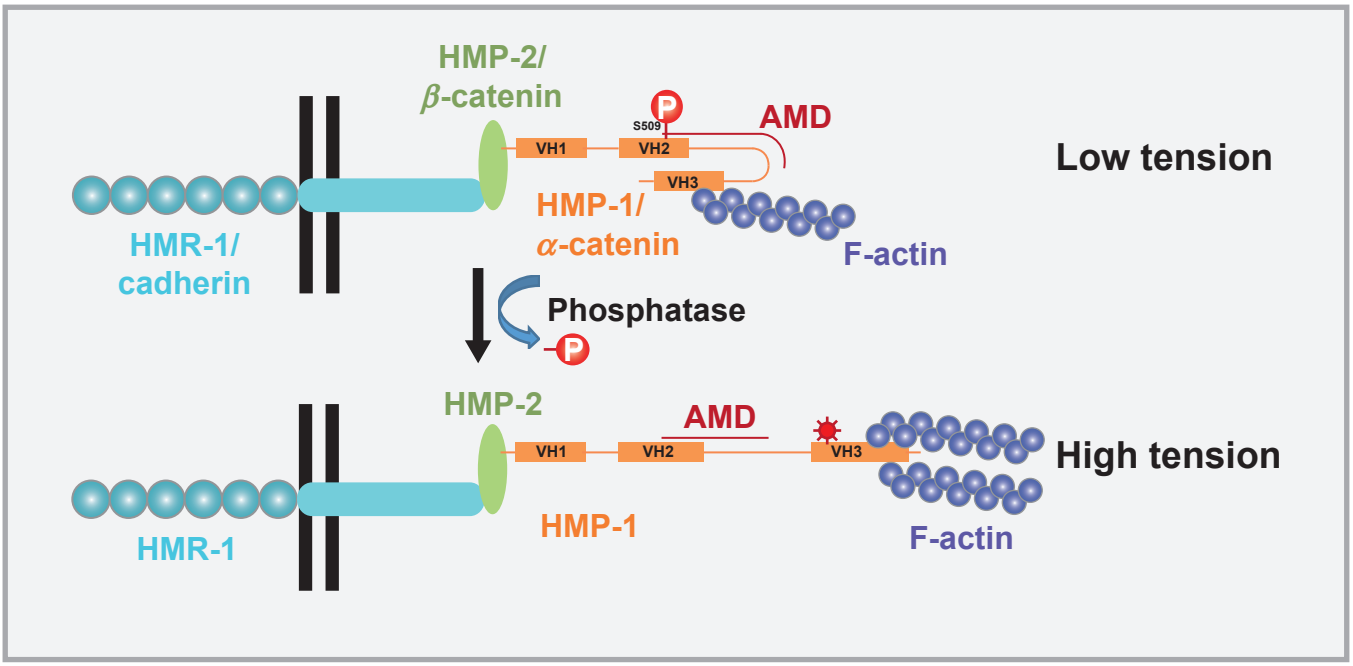
HMP-2/
β-catenin
S509
AMD
VH1
VH2
VH3
Low tension
HMR-1/
cadherin
HMP-1/
α-catenin
F-actin
Phosphatase
HMP-2
AMD
VH1
VH2
VH3
High tension
HMR-1
HMP-1
F-actin

Figure S5